Influence of the boundary condition on the first ply failure and stress distribution on a multilayer composite pipe by the finite element method.

Juan León Becerra, Octavio Andrés González-Estrada, Alberto Pertuz

Influence of the boundary condition on the first ply failure and stress distribution on a multilayer composite pipe by the finite element method.

Influencia de la condición de contorno en el fallo de la primera capa y la distribución de esfuerzos en una tubería de material compuesto multicapa por el método de elementos finitos.

S. León Becerra[1a], O.A. González-Estrada[1b], A. Pertuz[1c]

[1]GIEMA, School of Mechanical Engineering, Universidad Industrial de Santander, Colombia.
Email: [a] juan.leon2@correo.uis.edu.co Orcid: 0000-0002-1740-3127, [b] agonzale@uis.edu.co, Orcid: 0000-0002-2778-3389, [c] apertuzc@uis.edu.co

ABSTRACT

In the present work we study the influence of the boundary conditions in the stress distribution and the first ply failure of a commercially available multilayer composite pipe using a finite element model. An ASTM D2290 standard test was performed in order to determine the ultimate tensile strength and burst pressure. Also, a tension test performed on a longitudinal strip of the pipe was used to evaluate the elasticity modulus. We compare the experimental results with the numerical model to validate the material model used in the approximation. Hoop and axial stresses were obtained for three different boundary conditions: open ends, fixed ends and closed ends. Diverse failure criteria were considered for the pipes in order to evaluate the first ply failure, and a comparison of failure criteria and boundary conditions was made.

KEYWORDS: Composite pipes, finite element analysis, simulation, failure criteria, pipe boundary condition.

RESUMEN

En el presente trabajo se estudia la influencia de las condiciones de contorno en la distribución de tensiones y el fallo de la primera capa de un tubo compuesto multicapa comercialmente disponible utilizando un modelo de elementos finitos. Se realizó una prueba estándar ASTM D2290 para determinar la resistencia a la tracción y la presión de estallido. También se utilizó una prueba de tensión realizada sobre una tira longitudinal de la tubería para evaluar el módulo de elasticidad. Comparamos los resultados experimentales con el modelo numérico para validar el modelo de material utilizado en la aproximación. Se obtuvieron tensiones circunferenciales y axiales para tres condiciones de contorno diferentes: extremos abiertos, fijos y cerrados. Se consideraron diversos criterios de falla para las tuberías con el fin de evaluar el fallo de la primera capa, y se hizo una comparación de los criterios de fallo y las condiciones de los límites.

PALABRAS CLAVE: Tubería compuesta, análisis por elementos finitos, simulación, criterios de falla, condición de contorno de tubería.

1. INTRODUCTION

During the last years, different types of composite pipes have been successfully used in the oil and gas fields mostly because their mechanical properties are very attractive, especially their weight to resistance ratio and their resistance to corrosion [1]. Other features such as ease of installation, high durability and ease of maintenance make them more desirable than steel pipes. Different studies on mechanical properties and laboratory tests have been carried out for their mechanical characterization [2]–[4].

Xia et al. [5], based on anisotropic tridimensional elasticity, gave an exact solution for the stresses and strains of an internal pressure pipe. This formulation was applied to the case of closed end pipes, however it is extensible to open end. There is not an analytical procedure to determine the stress distribution on a fixed ends boundary condition.
Lekhnistskii [6] defined relations for the problem of plane stress in a cylindrical shell. Later, Tsai [7] included the plane strain (axial force different from zero). The material resistance was evaluated by two methods: first ply failure and last ply failure. Kanter et al. [8] investigated an analytical tool for composite thermoplastic pipes with the objective of correlating the results with laboratory tests such as tension, compression, internal and external pressure. Bakaiyan et al. [9] analyzed composite pipes exposed to thermomechanical loads because of the hot fluid circulating inside them, which can create temperature gradients.

Quintero Ortiz et al. [4] examined the effect of scratches on the surface of composite pipelines for the transportation of hydrocarbons by experimental means. Soden et al. [10] performed rupture tests with tubular samples of epoxy glass fiber laminates, with 60% resin and ± 55 ° winding angles. Strain-stress curves showed nonlinear behavior. Ferry et al. [11] showed that pipes exhibit varying types of damaged elastoplastic behavior depending on stress ratio axial stress/hoop stress. The extent of damage and plastic phenomena are responsible for non-linearity on stress-strain curves. They showed by micrographic analysis that micro cracking is the main damaging process.

Reutov [12] studied, using finite elements, the multilayer pipes stress distribution for Oil & Gas applications, obtaining the equivalent stresses for each layer, where it was determined that the middle reinforced layer presents the maximum stresses for operation pressures. Bai et al. [13] investigated a mathematical and numerical model to analyze the collapse of the RTP pipeline, the results of the simulation with FEM reflected a very minimal error percentage with respect to the theoretical analysis. Yu et al. [14] performed numerical analysis studies on reinforced thermoplastic pipes (RTP) with aramid fiber. The results related the buckling failure with the angles between the reinforcement layers. De Sousa et al. [15] obtained results of stresses for the composite pipe type Riser, containing metallic and thermoplastic layers, from theoretical and numerical models. Anping et al. [16] performed a finite element analysis (FEA) to determine the mechanical properties of two types of composite pipes reinforced with steel wires.

Onder et al. [17] subjected a GRP pipe to internal pressure under closed end condition, and burst strength is evaluated by analytical, FEA and experimental techniques. The Tsai-Wu criterion, the maximum stress and the maximum strain theories were used to compute the burst failure pressure of the composite layers in a simple form. The FEM method does not give an accurate burst pressure because strength reduction is not taken into account, just the first ply failure.

Vedvik et al. [18] conducted an analysis for thick walled composite pipes with an isotropic liner, special attention was given to the process of damage. The research accounted for damage in the composite layer and plastic yielding in the isotropic layer.

In this work, the effect of the boundary conditions on the hoop and axial stresses is investigated for a commercially available pipe of reinforced fiberglass (Fiberspar®). A first ply failure pressure is obtained for each boundary condition according to different failure criteria. First, in section 2 the elasticity model which defines the mechanical behavior of the pipe is presented. In section 3 the parameter adjustment by experiments is done and the simulation is carried out. Results and discussion are presented in section 4 and, finally, section 5 shows the conclusions.

2. ELASTICITY MODEL FOR COMPOSITE PIPES

Flexible composite pipes of filament winding technology have anisotropic behavior due to the different angles of the reinforcing layers. The pipes are characterized by having a low bending stiffness compared to steel pipes.

The Fiberspar® pipe consists of 3 main layers [19]: PE 3408 high density polyethylene, inner and outer layer, and an middle layer which is an Epoxy E glass fiber reinforcement, Figure 1.

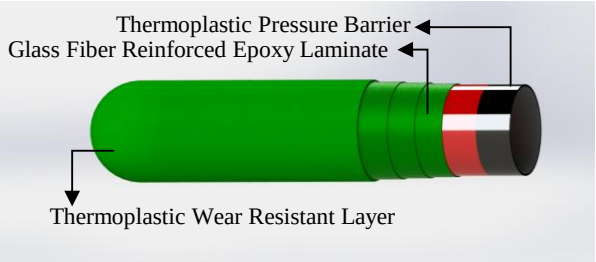

Figure 1. Fiberspar® pipe, construction model.

2.1. Strenght in composite pipes

Kaynak et al. [20] performed tests in accordance with ASTM D2290 standard for composite spoolable pipes, with glass or carbon fibers bonded with epoxy resin, in order to measure the ultimate tensile strength. A strong dependence of the tangential tensile strength and modulus of elasticity with respect to the winding angle was observed (see Figure 2. Hoop tensile strength for different winding angles. Epoxy E-glass wet.).

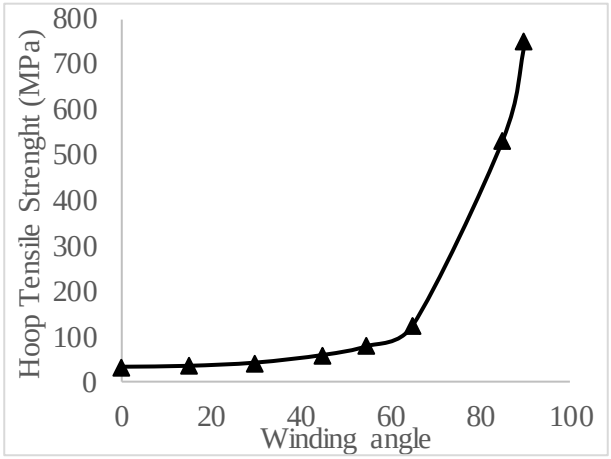

Figure 2. Hoop tensile strength for different winding angles. Epoxy E-glass wet.

Carroll et al. [21] conducted an experimental study of fiberglass with epoxy tubes with ± 55º winding angles with internal diameter of 2 in. A test machine was used which allows different radial and axial load ratios. The resulting stress-strain curves showed a complex behavior of the tubes.

The behavior in the fiberglass pipes is elastic-linear at the beginning, followed by a non-linear behavior near the fault, first by small leaks and second by ruptures. Generally, the nonlinear response is due to the formation of cracks in the matrix [22].

2.2. Elasticity model for composite materials

Consider the stress vector $\boldsymbol{\sigma} = \{\sigma_{xx}, \sigma_{yy}, \sigma_{xy}\}^{\boldsymbol{T}}$, displacements $\mathbf{u}$ and

strains $\boldsymbol{\varepsilon}$, defined on the domain $\Omega \subset \mathbb{R}^2$. Let us take **b** as the volumetric loads, **t** the Neumann tractions and $\bar{\mathbf{u}}$ the Dirichlet conditions. The elasticity problem is defined as finding **u** such that it satisfies:

$$\mathbf{L}^{\mathrm{T}}\boldsymbol{\sigma} + \mathbf{b} = 0 \text{ in } \Omega \quad (1)$$

$$\mathbf{G}\boldsymbol{\sigma} = \mathbf{t} \text{ in } \Gamma_{\mathrm{N}} \quad (2)$$

$$\mathbf{u} = \bar{\mathbf{u}} \text{ in } \Gamma_{\mathrm{D}} \quad (3)$$

$$\boldsymbol{\varepsilon}(\mathbf{u}) = \mathbf{L}\mathbf{u} \quad (4)$$

$$\boldsymbol{\sigma} = \mathbf{C}\boldsymbol{\varepsilon}(\mathbf{u}), \quad (5)$$

Where **L** is a differential operator, **G** is an operator that projects the stresses for equilibrium in the contour and **C** is the elasticity matrix of the material.

The above problem expressed in its variational form is written: Find $\mathbf{u} \in \mathbf{V}$ "such" that $\forall$ v $\in$ **V**:

$$\int_{\boldsymbol{\Omega}} \boldsymbol{\varepsilon}(\mathbf{v})^{\mathbf{T}}\mathbf{D}\boldsymbol{\varepsilon}(\mathbf{u})\mathrm{d}\Omega = \int_{\boldsymbol{\Omega}} \mathbf{v}^{\mathrm{T}}\mathbf{b}\,\mathrm{d}\Omega + \int_{\boldsymbol{\Gamma}_{\mathbf{N}}} \mathbf{v}^{\mathrm{T}}\mathbf{t}\;\mathrm{d}\Gamma, \quad (6)$$

where $\boldsymbol{V} = \{\mathbf{v} | \mathbf{v} \in [\mathbf{H}^1(\boldsymbol{\Omega})]^2, \mathbf{v}_{\boldsymbol{\Gamma}} = \mathbf{0}\}$.

Considering the orthogonal planes of symmetry of the model, the material is orthotropic. The stress strain relationship of the constitutive law in (5) can be expressed in terms of the stiffness matrix C as:

$$\begin{Bmatrix} \sigma_x \\ \sigma_y \\ \sigma_z \\ \tau_{yz} \\ \tau_{xz} \\ \tau_{xy} \end{Bmatrix} = [\mathbf{C}] \begin{Bmatrix} \varepsilon_x \\ \varepsilon_y \\ \varepsilon_z \\ \gamma_{yz} \\ \gamma_{xz} \\ \gamma_{xy} \end{Bmatrix} \quad (7)$$

$$[\mathbf{C}] = \begin{bmatrix} C_{11} & C_{12} & C_{13} & 0 & 0 & 0 \\ C_{21} & C_{22} & C_{23} & 0 & 0 & 0 \\ C_{31} & C_{32} & C_{33} & 0 & 0 & 0 \\ 0 & 0 & 0 & C_{44} & 0 & 0 \\ 0 & 0 & 0 & 0 & C_{55} & 0 \\ 0 & 0 & 0 & 0 & 0 & C_{66} \end{bmatrix}$$

Where the behavior of the material can now be defined by 9 independent constants. The constants C_{ij} are obtained from the classical theory of laminates considering the elastic properties of the fiber and matrix. It can be seen that the angular deformations and the longitudinal deformations are decoupled from the normal stresses and the tangential stresses, respectively, due to the null terms. Furthermore, there is no interaction between the tangential stresses and the angular deformations in the different planes.

2.2.1. Finite element solution.

For a discretization using a standard finite element (FEM) formulation in the elasticity problem, we find the solution $\mathbf{u}^{\mathrm{h}} \in \mathbf{V}^{\mathrm{h}}$ such that $\forall \mathbf{v} \in \mathbf{V}^{\mathrm{h}}$:

$$\int_{\Omega} \boldsymbol{\varepsilon}(\mathbf{v})^{\mathrm{T}}\mathbf{D}\boldsymbol{\varepsilon}(\mathbf{u}^{\mathrm{h}})\mathrm{d}\Omega = \int_{\Omega} \mathbf{v}^{\mathrm{T}}\mathbf{b}\,\mathrm{d}\Omega + \int_{\Gamma_{\mathrm{N}}} \mathbf{v}^{\mathrm{T}}\mathbf{t}\;\mathrm{d}\Gamma. \quad (8)$$

The above problem is solved using the classical finite element theory [23], resulting in the linear system $\mathbf{KU} = \mathbf{F}$, where **K** is the stiffness matrix, **U** is the displacement vector, and **F** is the vector of equivalent forces.

2.2.2. Plane stiffness of symmetrical laminates

A laminate is a set of plies stacked on top of one another and which, in its manufacturing process, ensures the continuity of the matrix in the direction orthogonal to the plane of the plies. In other words, each ply works in conjunction with the others.

One type of laminate stacking that is often used, and which corresponds to the model of the simulated pipe, are the so-called symmetrical laminates. A laminate is symmetrical when the sequence of stacking of the plies on either side of the median plane are identical.

The properties in the direction of the fiber differ from the properties in the direction of the main axes of the cylinder (axial, radial, and circumferential). To identify the properties of the pipe it is necessary to know and establish the relationships with respect to the directions of the composite material. It is convenient to use two coordinate systems: one to define the local axes (1, 2) whose first direction coincides with the fiber direction, and another to define the global axes (*x, y, z*).

Given the geometrical characteristics of the ply, a plane stress state is assumed. The stress strain relation for a unidirectional ply can be expressed as a function of the flexibility matrix $\mathbf{S} = \mathbf{C}^{-1}$ as:

$$\begin{Bmatrix} \varepsilon_1 \\ \varepsilon_2 \\ \gamma_{12} \end{Bmatrix} = \begin{bmatrix} S_{11} & S_{11} & 0 \\ S_{11} & S_{11} & 0 \\ 0 & 0 & S_{11} \end{bmatrix} \begin{Bmatrix} \sigma_1 \\ \sigma_2 \\ \tau_{12} \end{Bmatrix} \quad (9)$$

$$= \begin{bmatrix} \frac{1}{E_1} & \frac{-\nu_{21}}{E_2} & 0 \\ \frac{-\nu_{12}}{E_1} & \frac{1}{E_2} & 0 \\ 0 & 0 & \frac{1}{G_{12}} \end{bmatrix} \begin{Bmatrix} \sigma_1 \\ \sigma_2 \\ \tau_{12} \end{Bmatrix}$$

where the components of the flexibility and stiffness matrices have been replaced by the corresponding relations with the elastic constants of the ply E_1, E_2, G_{12}, ν_{12}, the values of which can be estimated from the properties of the constitutive materials.

Each ply orientation uses a local coordinate system, and it is necessary to refer the individual response of each ply to the global coordinate system and vice versa. For the transformation of the components of stress and strain between the systems of coordinates of global equations and those of the composite material, the matrix of rotation of stresses is used:

$$\begin{Bmatrix} \sigma_1 \\ \sigma_2 \\ \tau_{12} \end{Bmatrix} = T_\sigma(\theta) \begin{Bmatrix} \sigma_x \\ \sigma_y \\ \tau_{xy} \end{Bmatrix}, \quad (10)$$

$$T_\sigma(\theta) = \begin{bmatrix} m^2 & n^2 & 2mn \\ n^2 & m^2 & -2mn \\ -mn & mn & m^2 - n^2 \end{bmatrix},$$

With $m = \cos\theta$ and $n = \sin\theta$. For the case of the strain a transformation matrix can be establish in a similar manner. The stress-strain relationships involve certain transformations contained in equation (11):

$$\begin{Bmatrix} \sigma_x \\ \sigma_y \\ \tau_{xy} \end{Bmatrix} = \quad (11)$$

$$T_\sigma^{-1}(\theta) \begin{bmatrix} Q_{11} & Q_{12} & 0 \\ Q_{21} & Q_{22} & 0 \\ 0 & 0 & Q_{66} \end{bmatrix} T_\varepsilon(\theta)$$

$$= \begin{bmatrix} \overline{Q}_{11} & \overline{Q}_{12} & \overline{Q}_{16} \\ \overline{Q}_{12} & \overline{Q}_{22} & \overline{Q}_{26} \\ \overline{Q}_{16} & \overline{Q}_{26} & \overline{Q}_{66} \end{bmatrix} \begin{Bmatrix} \varepsilon_x \\ \varepsilon_y \\ \gamma_{xy} \end{Bmatrix}$$

In an analog manner it is possible to obtain the strain as a function of the applied stress. The

matrices $\bar{Q}$ and $\bar{S}$ are the so-called transformed (or not oriented) reduced matrices of rigidity and flexibility, respectively, referenced now in global axes.

2.3. Failure criteria

The composites are not homogeneous, anisotropic and brittle. This determines the different failure modes of the material, some related to the failure of the constituents and other to the interface [24].

In the fibers, two different failure modes can be considered: related to a tensile load and related to a compressive load. A characteristic of the fiber is that it does not usually show plastic deformation, the failure is related to a phenomenon of redistribution of stresses to the neighboring fibers. This redistribution may cause a new fiber rupture. In the case of a compressive charge, the progressive micro buckling of the fibers takes place until the fibers break.

In the matrix, microcracking is the main mode of failure. This is equivalent to matrix cracks parallel to the fiber direction over the entire thickness of the ply and especially to those plies where the reinforcement is not in the same direction as the applied load.

Another mode of common failure is the disunion, which equals a loss of adhesion and a relative slip between the fiber and the matrix due to differences in shear stresses at the fiber-matrix interface [25].

For the design with composite materials, it is common practice to evaluate interactive failure criteria that take into account the interactions of the stresses.

2.3.1. Maximum stress and maximum strain criteria.

A ply fails if [26]:

$$\begin{aligned} \sigma_1 \geq \mathrm{X}_1^{\mathrm{T}} \quad \sigma_1 \geq -\mathrm{X}_1^{\mathrm{C}} \\ \sigma_2 \geq \mathrm{X}_2^{\mathrm{T}} \quad \sigma_2 \geq -\mathrm{X}_1^{\mathrm{C}} \\ \sigma_{12} \geq S \quad \sigma_{12} \geq -\mathrm{S} \end{aligned} \tag{12}$$

Where $\mathrm{X}_i^{\mathrm{T}}$ represents the uniaxial tensile strength of the ply in the *i* direction, $\mathrm{X}_i^{\mathrm{C}}$ is the uniaxial compressive strength in the *i* direction, and S the shear strength in the plane. σ_1, σ_2 and σ_{12} represent the stress components in the 1-2 coordinate system.

In an analog manner, the maximum strain criterion establishes that the ply fails if the strain is above a permissible strain. No interaction between different failure modes is permitted in this two approaches.

2.3.2. Tsai-Hill criterion.

This is a criterion based on the polynomial failure criterion and is one of the most used criteria, and with results more adjusted to experimental values [24], [27]. The Tsai-Hill criterion reads

$$\left(\frac{\sigma_1}{\mathrm{X}_1^{\mathrm{T}}}\right)^2 + \left(\frac{\sigma_2}{\mathrm{X}_2^{\mathrm{T}}}\right)^2 + \left(\frac{\sigma_{12}}{\mathrm{S}}\right)^2 - \left(\frac{\sigma_1\sigma_2}{\mathrm{X}_1^{\mathrm{T}}}\right) \leq 1, \tag{13}$$

where the failure will occur for values greater than one. The disadvantage of Tsai-Hill is that it does not differentiate between strength to tension failure and compression during evaluation. In the case of compressive stresses, the compressive strengths are used in (13).

2.3.3. Tsai-Wu criterion.

Based on the Beltrami total energy deformation failure theory, for plane stress condition the failure is determined by the following expression [24], [27]:

$$f_1\sigma_1 + f_2\sigma_2 + f_{11}\sigma_1^2 + f_{22}\sigma_2^2 + 2f_{12}\sigma_1\sigma_2 + f_{66}\sigma_{12}^2 \geq 1 \quad (14)$$

Where $f_1, f_2, f_{11}, f_{22}, f_{66}$ are parameters described in terms of the ultimate strengths in the principal directions and f_{12} is determined experimentally with a biaxial stress test. Tsai-Wu is widely used in the analysis of progressive damage models for laminates since it allows to determine three-dimensional failure with a unique expression.

2.3.4. Hashin criterion

In [28], the authors indicated that it is not evident that all distinct failures modes could be expressed by a single function such as the foregoing criteria. They identified two mechanisms of failure: in the fiber and in the matrix, and provided expressions to identify each failure by considering separately traction and compression. For plane stress conditions the expressions read:

Tensile fiber mode

$$\left(\frac{\sigma_1}{X_1^T}\right)^2 + \left(\frac{\sigma_{12}}{S}\right)^2 = 1, \quad (15)$$

Fiber compressive mode

$$\left(\frac{\sigma_1}{X_1^C}\right)^2 = 1, \quad (16)$$

Tensile matrix mode

$$\left(\frac{\sigma_2}{X_2^T}\right)^2 + \left(\frac{\sigma_{12}}{S}\right)^2 = 1, \quad (17)$$

Compressive matrix

$$\left(\frac{\sigma_2}{2X_4}\right)^2 + \left[\left(\frac{X_2^C}{2X_4}\right)^2 - 1\right]\left(\frac{\sigma_2}{X_2^C}\right)^2 + \left(\frac{\sigma_{12}}{S}\right)^2 = 1, \quad (18)$$

where X_4 is the transverse failure shear.

2.3.5. Hoffman criterion

To take into account the effects of isotropic stress in the Hill's equation for orthotropic materials, Hoffman [29] included terms that are linear in the stress. The failure criterion for plane stress is then described by the equation [30]:

$$-\frac{\sigma_1^2}{X_1^T X_1^C} + \frac{\sigma_1\sigma_2}{X_1^T X_1^C} - \frac{\sigma_2^2}{X_2^T X_2^C} + \frac{X_1^T + X_1^C}{X_1^T X_1^C}\sigma_1 + \frac{X_2^T + X_2^C}{X_2^T X_2^C}\sigma_2 + \frac{\sigma_{12}^2}{S^2} = 1. \quad (19)$$

3. EXPERIMENTATION AND SIMULATION

The Fiberspar® pipe in its catalog has a variety of operating conditions, ranging from 5.17 MPa (750 psi) to 17.23 MPa (2,500 psi), these pressures are known as nominal pressure or operating pressure. The simulated pipe is a 50.8 mm nominal diameter pipe and 5.17 MPa as operating pressure. Piping burst tests for this model have ranged from 27.17 MPa (3,940.6 psi) to 31 MPa (4,800 psi).

Two experimental procedures were performed. First, the apparent hoop tensile stress, done by the ASTM D-2290, was done in order to obtain the ultimate stresses or burst pressure. Then, a tension test on a strip cut from a

multilayer pipe was performed to obtain the elastic properties. Finally, a simulation using the above parameters was performed on a complete pipe and under three different boundary conditions [11] to obtain the first ply failure and the stress distribution.

3.1. Apparent hoop tensile stress

In order to obtain the ultimate strength of the material, a tensile strength test was performed in the laboratory to obtain values of apparent normal stress under ASTM D-2290 [31], using a split ring segment. The specimen is a pipe sample as shown in Figure 3. Geometry of the ASTM D2290 test specimen [32]. This test allows to obtain an apparent ultimate hoop stress at which it occurs the pipe burst.

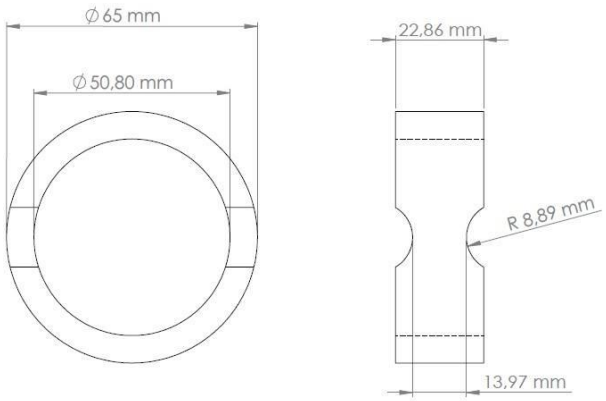

Figure 3. Geometry of the ASTM D2290 test specimen [32].

The average ultimate hoop stress is 81.44 MPa, with a standard deviation of 7.81 MPa. For the numerical model of the test, a half pipe is modeled by considering the conditions of symmetry.

Figure 4. Normal stress view in the stress concentration zone [32]. shows the results of the hoop stress presented on the pipe, which for the cross section considered coincides with the normal tension. The apparent stress calculated on the minimum sample area corresponds to 82.312 MPa, the error between the experimental test and the numerical model is 1.06%. These results help to validate the material model and the numerical model for the commercial pipe.

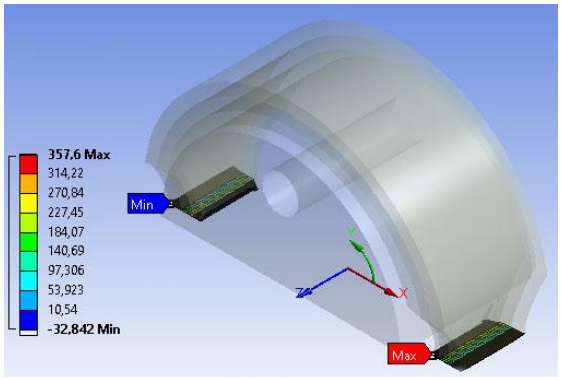

Figure 4. Normal stress view in the stress concentration zone [32].

3.2. Tension test

To obtain the values of the elastic constants, a tension test was also performed in a MTS Bionix uniaxial test machine, see Figure 5. MTS Bionix uniaxial test machine A finite element analysis of the strip was done, and the elastic properties were adjusted, until good agreement was found between the FE model and the experiment.

Layer	Young´s Modulus			Poisson Ratio			Shear Modulus		
	E_1 [MPa]	E_2 [MPa]	E_3 [MPa]	ν_{12}	ν_{23}	ν_{13}	G_{12} [MPa]	G_{23} [MPa]	G_{13} [MPa]
Interior HDPE	1340	/	/	0,4	/	/	478,5	/	/
Epoxy-glass fiber laminate	35000	9000	9000	0,28	0,4	0,28	4700	3500	4700
Exterior HDPE	1340	/	/	0,4	/	/	478,5	/	/

Table 1. Physical properties of the simulated composite pipes layers

Figure 5. MTS Bionix uniaxial test machine

The normal stresses show a homogenous distribution over almost all the length, however, near the traction surfaces the stresses are higher. This explains the zone of failure in Figure 6. Experimental and numerical model of the longitudinal strip. To give an example, the displacement obtained with a 2,500 N load by FE was 0.372 mm and experimentally it was 0.353, just about a 5% error.

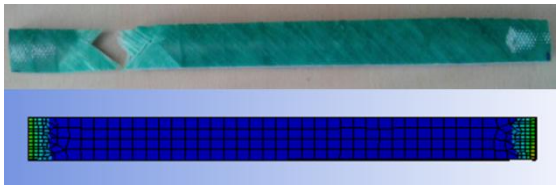

Figure 6. Experimental and numerical model of the longitudinal strip

3.3. Numerical model

This section describes the finite element numerical approximation for a multilayer composite pipe subjected to internal pressure. It defines the material model and the different boundary conditions used for the analysis of the stresses and first ply failure.

3.3.1. Dimensions and model of the material.

For the definition of the geometric model, Table 2 shows the dimensions of the constituent layers.

Layer	Internal Diameter [mm]	External Diameter [mm]
Interior HDPE	50.8	55.78
Epoxy-glass fiber laminate	55.78	59.79

Exterior HDPE	59.79	64.77

Table 2. Geometric characteristics of the layers of the Fiberspar® pipe.

The reinforcement laminate is composed of 4 stacked plies with orientations of ± 55 °, the configuration is [55/-55/55/-55]. Each ply has a thickness of 0.02 in (0.502 mm)

The mechanical properties of the layers used in the simulation are shown in Table 1. Physical properties of the simulated composite pipes layersThe results for Young's modulus, Poisson's coefficients and shear stiffness moduli for the reinforcement layer correspond to the values calculated from classical theory of laminates and obtained experimentally, as indicated in the previous sections. In the table, the subscript 1 indicates the direction of the fiber, the subscript 2 indicates the direction transverse to the fiber and the subscript 3 refers to the direction perpendicular to the plane 12.

3.3.2. Mesh

In order to control the discretization error, a sensitivity analysis of the mesh was performed. The results are shown in Figure 7. Convergence of the stresses on the epoxy-fiberglass layer The refinement was performed for the reinforcement layer until a variation of the hoop stress of less than 1% was obtained. The mesh is made with order two hexahedral elements for the epoxy-fiberglass layer and for the inner and outer layers of polyethylene. Linear contact conditions were defined between the layers.

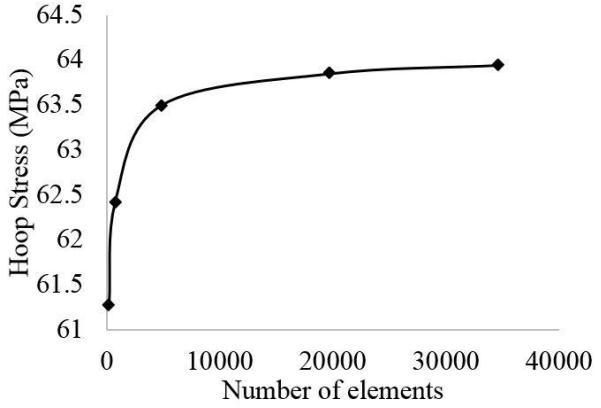

Figure 7. Convergence of the stresses on the epoxy-fiberglass layer

The last mesh for the pipeline contains 74,112 elements and 241,215 nodes.

3.3.3. Boundary conditions at nominal working pressure.

Three boundary conditions were tested: (i) open end condition, in which it does not exist longitudinal stresses, this condition generally applies on pipes subjected to very elastic supports, (ii) fixed ends, in which the axial displacements in the ends are restricted in the normal direction, this is the case of very long pipes or pipes with fixed flanges and (iii) closed ends, condition known as pressure vessel condition [33]. An internal pressure of 5.17 MPa (750 psi) was applied in all cases.

For the open end condition, the displacement in the axial direction of one end was restricted and a tiny axial load was set in the other end. The closed end condition was simulated putting two axial forces equivalent to the forces of the pressure acting on the ends. The fixed end condition was simulated using an axial displacement restriction in both ends.

4. RESULTS & DISCUSSION

4.1. Stresses at nominal working pressure.

For the nominal working pressure of 5.17 MPa (750 psi), the main maximum stresses obtained are presented on the glass fiber reinforcement layer generating a maximum hoop stress of 61.4 MPa, (the hoop stress distribution is the same regardless the boundary condition). The hoop stresses in the outer layer of HDPE were greater than those of the inner layer, see Figure 8. Hoop stress distributions.

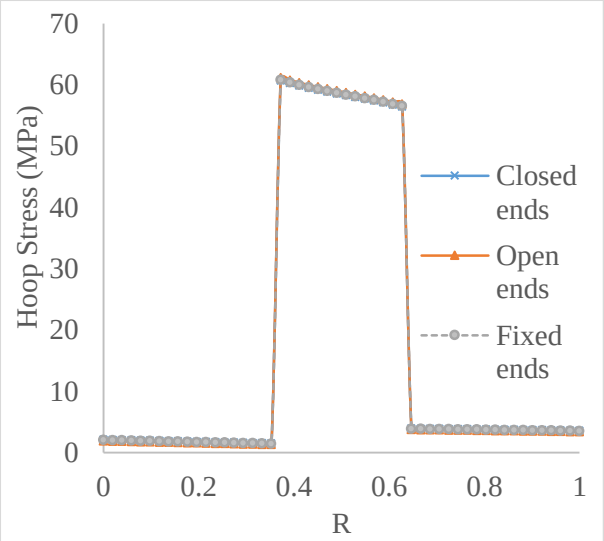

Figure 8. Hoop stress distributions.

The deformation analysis shows that the layer with the greatest deformation is the inner polyethylene with a deformation value along the ring of 0.018 mm / mm and a minimum value in the outer layer of 0.01 mm / mm. For a fixed end conditions. This condition holds true for the other two boundary conditions.
The results indicate that the ply of fiberglass composite closest to the inner layer presents greater stress and this decreases linearly towards the last layer. Reflecting how the stress is largely assumed by the laminate layer. The polyethylene layers work to protect the laminate layer from corrosion and transmit the greatest stresses to the composite laminate.

The Figure 9 shows the distribution of the axial stresses across the dimensionless radius, it is observed that the open end boundary condition sustains the smallest value of stress for any point across the thickness, fixed ends follows and the closed ends is the highest.

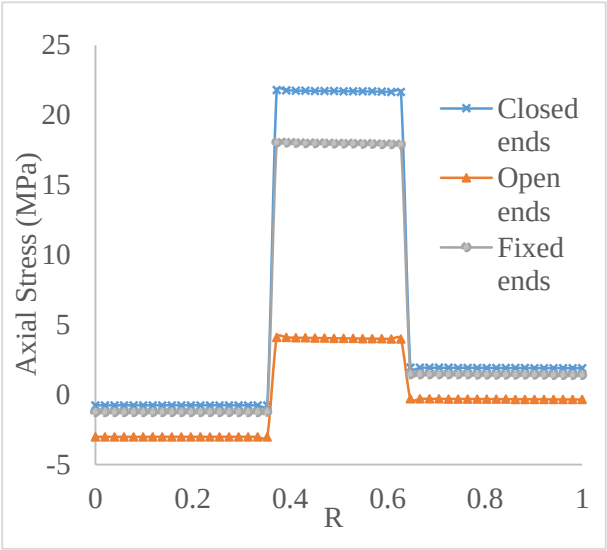

Figure 9. Axial stresses on the pipe as a function of the dimensionless radius

4.2. First ply failure.

Using the different failure criteria, it is confirmed that for a working pressure of 5.17 MPa there is no ply failure. The load was increased until the first ply failure is obtained, the results are shown in Table 3. FPF pressure for different failure criteria In all cases, the first inner ply is the most critical, there may be fiber rupture or matrix micro cracking rather than a complete failure of the pipe. The analysis performed for a pressure of 27 MPa confirms that there is failure of all the plies.

First Ply Failure Pressure Condition			
Failure criteria	**Open end [MPa]**	**Fixed end [MPa]**	**Closed end [MPa]**
Max stress	13.73	11.15	9.25
Max strain	16.13	14.97	9.96
Tsai-Hill	10.94	9.96	8.62
Tsai-Wu	10.87	10.70	9.41
Hoffman	10.48	10.06	8.82
Hashin	11.06	10.04	8.68

Table 3. FPF pressure for different failure criteria

It is observed that the maximum stress and maximum strain shows the highest values of FPF pressure, this is due to the fact that this criterion does not take into account the stress interaction, the other criteria exhibit a lower FPF pressure and similar values between them. In regard of the boundary condition, it is observed that the one that supports the highest pressure is the open end condition also called pure internal pressure.

This FPF pressure is nearly twice as double of the nominal pressure, and nearly half of the final burst pressure, however a burst pressure is not possible to obtain in this model because it does not take into account for a material degradation model.

5. CONCLUSIONS

The composite model for the Fiberspar® tubing was numerically defined. Particular interest was given in the definition of the fiber reinforced layer, and the model was validated through experimental tests. The error between the results of the laboratory test according to ASTM D2290 and the tension model with the numerical approximation is minimal. This validates the parameters used to define the computational model of the material.

It can be seen that when the orthotropic pipe is subjected to a pressure greater than 10 MPa the first epoxy-fiberglass plies fails, but this does not mean that the pipe fails completely. At a burst pressure of 27.17 MPa the pipe fails on all the plies, and this point is called functional failure.

The values of the stresses on the pipe were determined for the three different boundary conditions when it works at its nominal pressure of 5.17 MPa. It was also found that the composite laminate layer is the one that withstands the greatest stresses with a value of 62 MPa for hoop stresses.

It was demonstrated that the FPF pressure for the open end or pure internal pressure condition was the highest, this is because in this conditions the axial stresses are the lowest compared to the other ones. Aditionally, the maximum strain and maximum stress criterion tends to over-estimate the FPF pressure because they do not take into account the interaction between axial and hoop stresses.

6. ACKNOWLEDGMENTS

This research was part of the project structural integrity of spoolable composite pipes by the ICP (Colombian Institute of Petroleum) code number 5222395.

7. REFERENCES

[1] R. Rafiee and A. Amini, “Modeling and experimental evaluation of functional failure pressures in glass fiber reinforced polyester pipes,” *Comput. Mater. Sci.*, vol. 96, no. PB, pp. 579–588, 2015.

[2] N. Ji, H. Geun, and J. Heum, “Structural analysis and optimum design of GRP pipes based on properties of materials,” *Constr. Build. Mater.*, vol. 38, pp. 316–326, 2013.

[3] D. Hull, “Research on composite materials at Liverpool University. I. Failure of filament wound tubes,” *Phys. Technol.*, vol. 13, no. 5, 1982.

[4] L. Amparo, Q. Ortiz, J. Ricardo, A. Villamizar, and A. Y. Vallen, “Efecto en las propiedades mecánicas de daños superficiales generados en tubería compuesta flexible para transporte de hidrocarburos,” vol. 39, pp. 39–48, 2015.

[5] M. Xia, H. Takayanagi, and K. Kemmochi, “Analysis of multi-layered filament-wound composite pipes under

internal pressure," *Compos. Struct.*, vol. 53, no. 4, pp. 483–491, 2001.

[6] S. Lekhnitskii, *Theory of elasticity of an anisotropic elastic body*. San Francisco : Holden-Day, 1963.

[7] S. W. Tsai, *Composite Design*, Fourth Edi. Dayton, OH: Think composites, 1988.

[8] J. L. C. G. de Kanter and J. Leijten, "Thermoplastic Composite Pipe: Analysis and Testing of a Novel Pipe System for Oil & Gas," in *Proceedings of the 17th ICCM*, 2009, pp. 1–10.

[9] H. Bakaiyan, H. Hosseini, and E. Ameri, "Analysis of multi-layered filament-wound composite pipes under combined internal pressure and thermomechanical loading with thermal variations," *Compos. Struct.*, vol. 88, no. 4, pp. 532–541, 2009.

[10] P. D. Soden, M. J. Hinton, and A. S. Kaddour, "Biaxial test results for strength and deformation of a range of E-glass and carbon fibre reinforced composite laminates. Failure exercise benchmark data," *Fail. Criteria Fibre-Reinforced-Polymer Compos.*, vol. 62, pp. 52–96, 2004.

[11] L. Ferry, D. Perreux, J. Rousseau, and F. Richard, "Interaction between plasticity and damage in the behaviour of [+φ, −φ]n fibre reinforced composite pipes in biaxial loading (internal pressure and tension)," *Compos. Part B Eng.*, vol. 29, pp. 715–723, 1998.

[12] Y. Reutov, "The calculation of multilayer polymer pipes using finite elements and their application to Gas and Oil pipelines," in *7th International Forum on Strategic Technology (IFOST)*, 2012, pp. 1–3.

[13] Y. Bai, J. Tang, W. Xu, Y. Cao, and R. Wang, "Collapse of reinforced thermoplastic pipe (RTP) under combined external pressure and bending moment," *Ocean Eng.*, vol. 94, pp. 10–18, 2015.

[14] K. Yu, E. V. Morozov, M. A. Ashraf, and K. Shankar, "Analysis of flexural behaviour of reinforced thermoplastic pipes considering material nonlinearity," *Compos. Struct.*, vol. 119, pp. 385–393, 2014.

[15] J. R. M. de Sousa, G. B. Ellwanger, and E. C. P. Lima, "Modelo tridimensional de elementos finitos para el análisis de esfuerzos de tubos flexibles," *Boletín Técnico*, vol. 42, no. 2, pp. 1–20.

[16] X. Anping, S. Peng, Z. Jingjing, and Q. Yunxia, "FEA-based Comparison of Two Kinds of Steel Wire Reinforced Composite Pipes," *4th Int. Conf. Intell. Networks Intell. Syst.*, pp. 184–187, 2011.

[17] A. Onder, O. Sayman, T. Dogan, and N. Tarakcioglu, "Burst failure load of composite pressure vessels," *Compos. Struct.*, vol. 89, no. 1, pp. 159–166, 2009.

[18] N. P. Vedvik and C. G. Gustafson, "Analysis of thick walled composite pipes with metal liner subjected to simultaneous matrix cracking and plastic flow," *Compos. Sci. Technol.*, vol. 68, no. 13, pp. 2705–2716, 2008.

[19] P. A. Quigley, S. C. Nolet, and J. G. Williams, "Composite spoolable tube," U.S. Patent 6,016,845, 2000.

[20] C. Kaynak, E. S. Erdiller, L. Parnas, and F. Senel, "Use of split-disk tests for the process parameters of filament wound epoxy composite tubes," *Polym. Test.*, vol. 24, no. 5, pp. 648–655, 2005.

[21] M. Carroll, F. Ellyin, D. Kujawski, and A. S. Chiu, "The rate-dependent behaviour of ± 55 ° filament-wound glass-fibre/epoxy tubes under biaxial loading," *Compos. Sci. Technol.*, vol. 55, no. 95, pp. 391–403, 1995.

[22] A. Majid and M. S. Bin, "Behaviour of composite pipes under multi-axial stress," Newcastle University, 2011.

[23] E. Carrera, *Theories and finite elements for multilayered, anisotropic, composite*

plates and shells, vol. 9, no. 2. 2002.
[24] M. Molinier, "Análisis de los criterios de falla aplicados a los laminados compuestos," Universidad de Buenos Aires, 2005.
[25] L. Arias Maya and L. Vanegas Useche, "Falla de los materiales compuestos laminados," *Sci. Tech.*, no. 25, pp. 113–118, 2004.
[26] E. J. Barbero, *Finite Element Analysis of Composite Materials Using ANSYS*, Second. Boca Raton, U.S.A.: CRC Press, 2013.
[27] M. E. Tuttle, *Structural Analysis of Polymeric Composite Materials*. New York, U.S.A., 2004.
[28] Z. Hashin, "Failure Criteria for Unidirectional Fibre Composites," *J. Appl. Mech.*, vol. 47, no. June, pp. 329–334, 1980.
[29] O. Hoffman, "Strength of Orthotropic Materials," *J. Compos. Mater.*, vol. 1, no. 1967, pp. 200–206, 1967.
[30] R. M. Jones, *Mechanics of composite materials*. Press, CRC, 1998.
[31] ASTM Standard, "ASTM 2290-12 Standard Test Method for Apparent Hoop Tensile Strength of Plastic or Reinforced," *ASTM B. Stand.*, pp. 1–8, 2016.
[32] O. A. González-Estrada, J. Leal Enciso, and J. D. Reyes Herrera, "Análisis de integridad estructural de tuberías de material compuesto para el transporte de hidrocarburos por elementos finitos.," *UIS Ing.*, vol. 15, no. 2, pp. 105–116, 2016.
[33] A. Onder, O. Sayman, T. Dogan, and N. Tarakcioglu, "Burst failure load of composite pressure vessels," *Compos. Struct.*, vol. 89, no. 1, pp. 159–166, 2009.